Numerical simulation of rheology of red blood cell rouleaux in microchannels

T. Wang,[1] T.-W. Pan,[1] Z. W. Xing,[2] and R. Glowinski[1]
[1]*Department of Mathematics, University of Houston, Houston, Texas 77204-3008, USA*
[2]*Department of Materials Science and Engineering, Nanjing University, Nanjing 210093, China*
(Received 8 September 2008; revised manuscript received 30 December 2008; published 17 April 2009)

An elastic spring model is applied to simulate the skeletal structure of the red blood cell (RBC) membrane and to study the dynamical behaviors of the red blood cell rouleaux (aggregates) in microchannels. The biconcave shape of RBCs in static plasma and the tank-treading phenomenon of single RBCs in simple shear flows have been successfully captured using this model. The aggregation and dissociation of RBCs with different deformability have been investigated in both shear and Poiseuille flows by taking into consideration the rheology of the cells and the intercellular interaction kinetics. It is found that the equilibrium configuration of the rouleaux formed under no-flow condition, the motion of the rouleaux in the flows, and the rheological behavior of individual cells in the rouleaux is closely related to the intercellular interaction strength, hydrodynamic viscous forces, and the deformability of the cell membrane.

DOI: 10.1103/PhysRevE.79.041916 PACS number(s): 87.16.dm, 87.18.Ed, 47.63.Cb

I. INTRODUCTION

Mathematical modeling of red blood cell (RBC) rheology and aggregation in microvessels (diameter <100 μm) has attracted growing interest recently. In the absence of external flow, a healthy RBC is a biconcave-shaped disk with a diameter of $6-8$ μm and a thickness of about 2 μm. The cell membrane is highly deformable so that RBCs can pass through capillaries of smaller diameter than the cells. Due to the presence of certain protein (such as fibrinogen and globulin) in blood plasma, RBCs may adhere together to form stack-of-coin-like rouleaux (aggregates). It is also observed that under pathological conditions, such as malaria, infected RBCs become more rigid and adhesive than healthy ones. The presence of massive rouleaux and the decrease in deformability of the cell membrane can impair the blood flow in microvessels and capillaries so that the amount of oxygen and nutrients that can be transported is severely reduced. Theoretical investigations of RBC rouleaux have been partly reviewed in [1,2]. Recent numerical studies on the RBC aggregation have taken into account the rheological aspect and dynamic motion of the cells in a flow [3–6]. A series of numerical studies have been carried out on the aggregates of two cells [3] and multiple cells [4–6]. The results suggested that rheological properties of the cells had significant effects on the dynamics of the aggregates [3] and the aggregation was linked to the shear rate dependent viscosity of the blood [5]. Very recently, a lattice Boltzmann method was developed by Zhang *et al.* [6] to simulate the formation and dissociation of four-cell rouleaux in shear flows. They showed that the configuration of the rouleaux formed under no-flow condition and the behaviors of the aggregates in shear flows depended strongly on the strength of the intercellular interaction and shear rate applied. These studies indicate that the aggregation of RBCs plays a significant role in the rheology and flow characteristics of blood. However, the rheological behavior of the aggregates related to the deformability of the cell membrane has been studied only to a limited extent. Moreover, blood flow in the microvessels is better approximated by a Poiseuille flow than a shear flow, which makes the study of RBCs in Poiseuille flows more physiologically realistic. In addition, although some important factors for the RBC aggregation and dissociation have been investigated [3–6], the determinant factors are complex and not well established.

Previous numerical studies depicted elastic properties of the RBC membrane by the Mooney-Rivlin strain energy function [4,5] or Neo-Hookean strain energy function [3,6] so that the deformability of the cells was included. However, the general organization of the RBC membrane has been well characterized. It has been shown that the human RBC is an inflated closed membrane filled with a viscous fluid called cytoplasma. The RBC membrane is a two-layer structure with one layer the phospholipid bilayer plus the attached glycocalyx and the other layer the network of proteins fastened to the bilayer [7,8]. The second layer is also called the skeleton of the membrane. The skeleton is a network of spectrin hexagons which allow the RBC to be highly deformable and elastic [9]. Due to its special structure, the RBC membrane has strong resistance to changes in area or volume and shear deformation [8]. Therefore, it is of significance to take into consideration the structure of the RBC membrane skeleton in the study of RBC aggregations. In this paper, a recently developed elastic spring model [10] based on the structure of the RBC membrane skeleton is adopted to describe the deformability of the RBCs, for this model is a more accurate representation of the cell membrane.

The goal of the present study is twofold. First, we aim to develop a numerical approach incorporated with the elastic spring model to study the rheology of the RBCs. Second, we focus on investigating the effect of cell mechanical properties, hydrodynamic forces, and strength of the intercellular interaction on the dynamical motion of the two-cell rouleaux. To this purpose, shear and Poiseuille flows including the RBC with fluid-cell and cell-cell interactions have been studied in two-dimensional (2D) microchannels using the numerical method developed and the simulation results are presented in this paper.

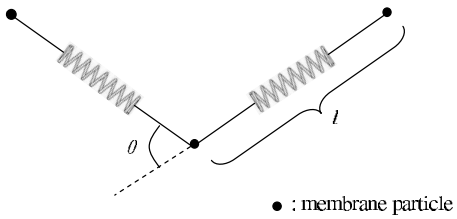

FIG. 1. The elastic spring model of the RBC membrane.

II. THEORY AND METHODS

Under the assumption that blood plasma is an incompressible Newtonian fluid, the governing equations for the blood flow in microvessels are the Navier-Stokes equations

$$\rho\left[\frac{\partial \mathbf{u}}{\partial t} + \mathbf{u}\cdot\nabla\mathbf{u}\right] = -\nabla p + \mu\Delta\mathbf{u} + \mathbf{f}, \tag{1}$$

$$\nabla\cdot\mathbf{u} = 0, \tag{2}$$

where $\mathbf{u}(\mathbf{x},t)$ and p are the fluid velocity and pressure, respectively, anywhere in the flow, ρ is the fluid density, and μ is the fluid viscosity, which is assumed to be constant for the entire fluid. The body force term $\mathbf{f}(\mathbf{x},t)$ is introduced to account for the force acting on the fluid or structure interface.

In this paper, the Navier-Stokes equations for fluid flow has been solved by a finite element technique. The aggregation and dissociation of RBCs in shear flows has been simulated by combining (1) a two-dimensional elastic spring model to describe the RBC membrane; (2) a Morse-type potential function to model the intercellular force; and (3) an immersed boundary method based on the Navier-Stokes equations to deal with the motion of the deformable cells.

A. Elastic spring model for the RBC membrane

The deformability and the elasticity of the RBC is due to the skeletal architecture of the membrane. A two-dimensional elastic spring model [10] is considered in this paper to describe the deformable behavior of the RBCs. Based on this model, the RBC membrane can be viewed as membrane particles connecting with the neighboring membrane particles by springs, as shown in Fig. 1. Elastic energy stores in the spring due to the change in the length l of the spring with respect to its reference length l_0 and the change in angle θ between two neighboring springs. The total elastic energy of the RBC membrane, $E=E_l+E_b$, is the sum of the total elastic energy for stretch or compression and the total elastic energy for bending which, in particular, are the following:

$$E_l = \frac{k_l}{2}\sum_{i=1}^{N}\left(\frac{l_i - l_0}{l_0}\right)^2 \tag{3}$$

and

$$E_b = \frac{k_b}{2}\sum_{i=1}^{N}\tan^2(\theta_i/2). \tag{4}$$

In Eqs. (3) and (4), N is the total number of the spring elements and k_l and k_b are spring constants for changes in length and bending angle, respectively. Based on the principle of virtual work, the elastic spring force acting on the membrane particle i is then

$$\mathbf{F}_i = -\frac{\partial E}{\partial \mathbf{r}_i}, \tag{5}$$

with $\mathbf{r}_i$ as the position of the ith membrane particle. For simulation purposes, this elastic force is a portion of the body force term in the Navier-Stokes equations.

B. RBC aggregation model

The underlying mechanism of RBC aggregation remains unclear at this time (bridging versus depletion). Descriptions of the bridging model and the depletion model can be found elsewhere [11,12]. Here we adopt a Morse-type potential function proposed by Liu *et al.* [4] for RBC adhesion phenomena to describe the intercellular energy between two cells

$$\phi(r) = D_e[e^{2\beta(r_0-r)} - 2e^{\beta(r_0-r)}], \tag{6}$$

where r is the distance considered, r_0 and D_e are reference distance and surface energy, respectively, and β is a scaling factor. The intercellular force is then $f(r)=-\partial\phi/\partial r$. The Morse-type potential function is chosen because of its simplicity. An accurate representation of intercellular interaction force is not central to this paper. Employing this potential function, the intercellular force is a weak depletion attractive at far distances and strong repulsive at near distances which qualitatively represents the characteristics of the interaction between the RBCs.

C. Immersed boundary method

The immersed boundary method developed by Peskin [13] is employed in this paper because of its distinguish features in dealing with the problem of fluid flow interacting with a flexible fluid or structure interface. Over the years, it has demonstrated its capability in the study of computational fluid dynamics including blood flow. Based on the method, the boundary of the deformable structure is discretized spatially into a set of boundary nodes. The force located at the immersed boundary node $\mathbf{X}$ affects the nearby fluid mesh nodes $\mathbf{x}$ through a 2D discrete δ function $D_h(\mathbf{X}-\mathbf{x})$,

$$\mathbf{F}(\mathbf{x}) = \sum \mathbf{F}(\mathbf{X})\cdot D_h(\mathbf{X}-\mathbf{x}) \quad \text{for} \quad |\mathbf{X}-\mathbf{x}| \le 2h, \tag{7}$$

where h is the uniform finite element mesh size and

$$D_h(\mathbf{X}-\mathbf{x}) = \delta_h(\mathbf{X}_1 - x_1)\delta_h(\mathbf{X}_2 - x_2), \tag{8}$$

with the one-dimensional (1D) discrete δ functions being

$$\delta_h(z) = \begin{cases} \dfrac{1}{4h}\left[1+\cos\left(\dfrac{\pi z}{2h}\right)\right] & \text{for } |z| \le 2h \\ 0 & \text{for } |z| > 2h. \end{cases} \tag{9}$$

The movement of the immersed boundary node $\mathbf{X}$ is also affected by the surrounding fluid and therefore is enforced by summing the velocities at the nearby fluid mesh nodes $\mathbf{x}$ weighted by the same discrete δ function,

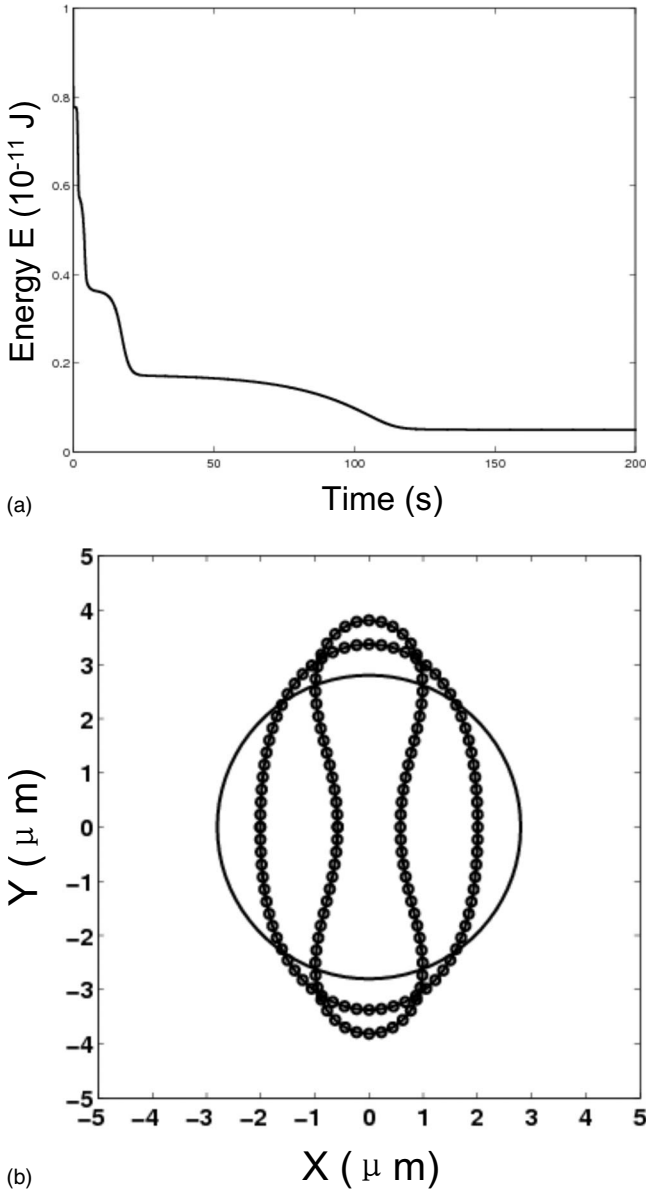

FIG. 2. (a) An example of the history of the change in the elastic energy of the RBC membrane. (b) Two-dimensional RBC shapes obtained by reducing the area from a circle using the elastic model. Elliptic shape: $s^*=0.9$; biconcave shape: $s^*=0.481$. The lines correspond to the RBC obtained from the elastic model, while the circles show the equilibrium RBC shape in a static blood plasma.

$$\mathbf{U}(\mathbf{X}) = \sum h^2 \mathbf{u}(\mathbf{x}) \cdot D_h(\mathbf{X} - \mathbf{x}) \quad \text{for} \quad |\mathbf{X} - \mathbf{x}| \leq 2h \tag{10}$$

After each time step Δt, the position of the immersed boundary node is updated by

$$\mathbf{X}_{t+\Delta t} = \mathbf{X}_t + \Delta t \mathbf{U}(\mathbf{X}_t). \tag{11}$$

III. NUMERICAL RESULTS AND DISCUSSIONS

In this paper, the RBCs are suspended in blood plasma which is assumed to be incompressible, Newtonian, and has a density of $\rho=1.00$ g/cm^3 and a dynamical viscosity of $\mu=0.012$ g/(cm s). The viscosity ratio which describes the viscosity contrast of the fluid inside and outside the RBC membrane is fixed at 1.0. The fluid domain is a two-dimensional horizontal channel. For all computations, the grid resolution for the computational domain is 80 grid points per unit length with the unit length equal to 10 μm. The reference distance r_0 in Eq. (6) is chosen to be 0.49 μm due to the limitation of the grid size. This distance can be further decreased provided a finer mesh grid is used. The scaling factor is picked as $\beta=80$ μm^{-1}. The energy constant D_e can be chosen differently so that a weak or strong intercellular interaction is introduced. To obtain a Poiseuille flow, a constant pressure gradient is prescribed as a body force. To produce a linear shear flow, a Couette flow driven by two walls at the top and bottom which have the same speed but move in directions opposite to each other is applied to the suspension. Different shear rate can be obtained by adjusting the wall speed. In addition, periodic boundary conditions are imposed at the left and right boundaries of the domain.

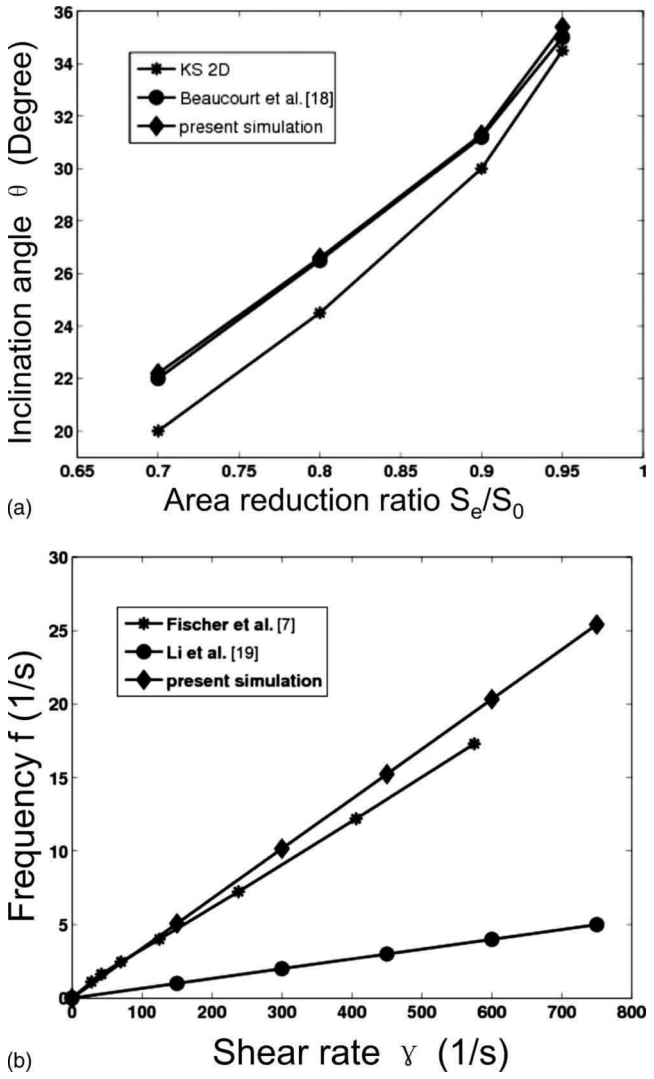

FIG. 3. (a) Equilibrium RBC inclination angle as a function of area reduction ratio. (b) Tank-treading frequency f as a function of shear rate in a fluid with viscosity $23cp$.

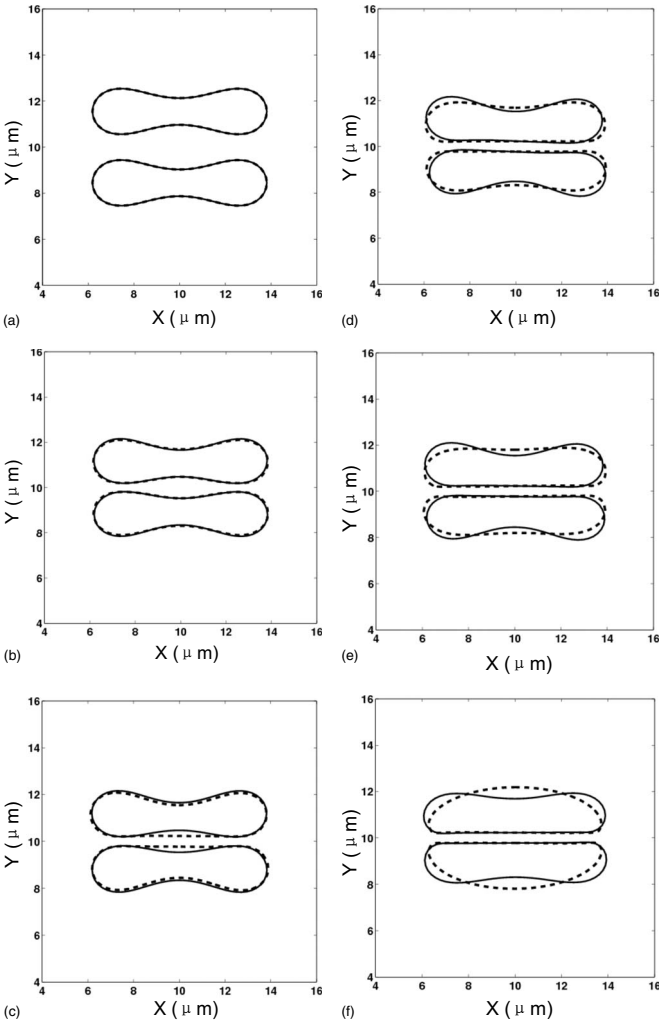

FIG. 4. Equilibrium configuration of RBC rouleaux with different intercellular strength. (a) $D_e=0$; (b) $D_e=1.0\times10^{-3}$ μJ/m^2; (c) $D_e=1.0\times10^{-1}$ μJ/m^2; (d) $D_e=5.5\times10^{-1}$ μJ/m^2; (e) $D_e=1.0$ μJ/m^2, and (f) $D_e=4.5$ μJ/m^2. Solid lines: $k_l=k_b=1.0\times10^{-12}$ N m; dashed lines: $k_l=k_b=1.0\times10^{-13}$ N m.

A. Shape change of a RBC

In many cases of interest, the two-dimensional model approximates the shape of the RBC by the characteristic cross section in the plane that is parallel to the flow direction if the cell were in shear flow. In previous studies, the shape of the RBC was either taken as an ellipse [3,14] or prescribed by an equation [4–6] suggested by Evans and Fung [15] for a biconcave shape. In this paper, the shape change of a RBC is simulated using the elastic spring model based on minimum energy principle. Initially, the RBC is assumed to be a circle with a radius of 2.8 μm. The circle is discretized into $N=76$ membrane particles so that 76 springs are formed by connecting the neighboring particles. The shape change is stimulated by reducing the total area of the circle s_0 through a penalty function [10],

$$\Gamma_s = \frac{k_s}{2}\left(\frac{s-s_e}{s_e}\right)^2, \tag{12}$$

and the total elastic spring energy E is modified as $E+\Gamma_s$, and the force acting on the ith membrane particle now is

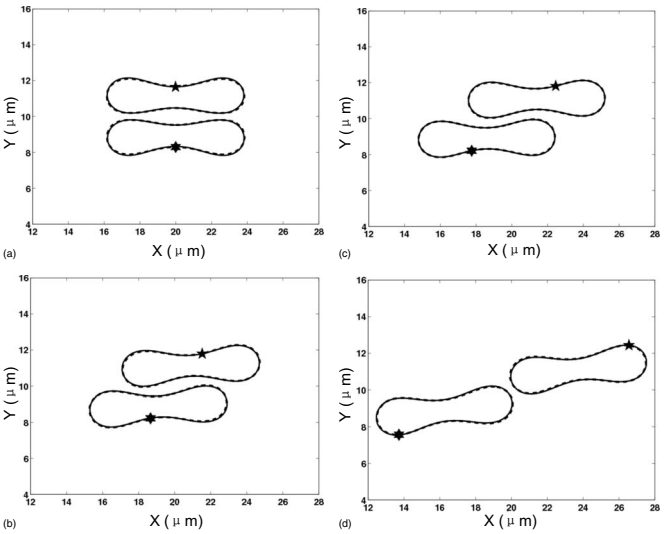

FIG. 5. Representation snapshots for the evolution of rouleaux of two cells in a shear flow with $\gamma=100$ s^{-1}. (a) $t=0$, (b) $\gamma t=1$, (c) $\gamma t=2$, and (d) $\gamma t=5$. The intercellular interaction between the two cells is weak with $D_e=1.0\times10^{-3}$ μJ/m^2. Solid lines: $k_l=k_b=1.0\times10^{-12}$ N m; dashed lines: $k_l=k_b=1.0\times10^{-13}$ N m.

$$\mathbf{F}_i = -\frac{\partial(E+\Gamma_s)}{\partial \mathbf{r}_i}, \tag{13}$$

where s and s_e are the time-dependent area and the equilibrium area of the RBC, respectively. When the area is reduced, each RBC membrane particle moves according to the following equation of motion:

$$m\ddot{\mathbf{r}}_i + \gamma\dot{\mathbf{r}}_i = \mathbf{F}_i. \tag{14}$$

Here, $\dot{(\,)}$ denotes the time derivative and m and γ represent the mass and the viscosity, respectively, of the RBC. The position $\mathbf{r}_i$ of the ith membrane particle is solved by a discrete analog of Eq. (14) via a second-order finite difference method. The total elastic energy stored in the membrane decreases as the time elapse. The final shape of the RBC shown in Fig. 2 is obtained as the total elastic energy is minimized.

The parameters in the simulation of the shape change of the RBCs are set as follows: the membrane mass $m=2.0\times10^{-4}$ g and the membrane viscosity $\gamma=8.8\times10^{-7}$ N s/m. By taking into consideration the nonextensible property of the membrane, the spring constants are set to be 1.0×10^{-13} and 1.0×10^{-12} N m, with $k_l=k_b$ for the more deformable cells (e.g., healthy cells) and less deformable cells (e.g., infected cells), respectively. The penalty coefficient k_s is $k_b\times10^4$. The bending constant is closely related to the rigidity of the membrane. A higher k_b results a less deformable cell. In Fig. 2, an initial circular shape is transformed into its final stable shape associated with a minimal energy for a given area ratio $s^*=s_e/s_0$ regardless the above choice of k_b. It is found that when the area reduction ratio $s^*\leq0.8$, biconcave shapes are obtained. When $s^*>0.8$, the final stable shape is close to ellipse. The biconcave shape obtained for $s^*=0.481$ resembles the normal physiological shape of the

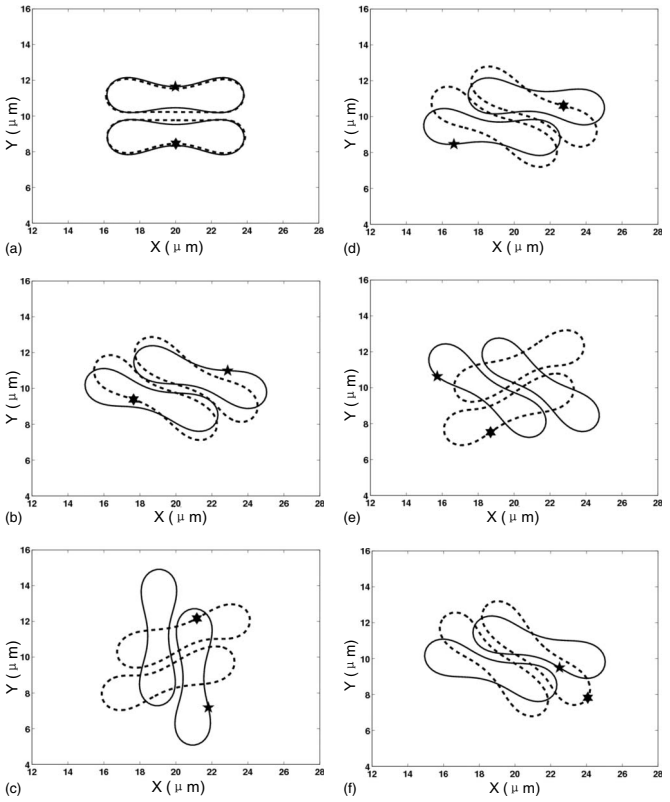

FIG. 6. Representation snapshots for the evolution of rouleaux of two cells in a shear flow with $\gamma=100\ s^{-1}$. (a) $t=0$, (b) $\gamma t=5$, (c) $\gamma t=10$, (d) $\gamma t=15$, (e) $\gamma t=20$, and (f) $\gamma t=77.8$. The intercellular interaction between the two cells is moderate with $D_e=1.0\times10^{-1}\ \mu J/m^2$. Solid lines: $k_l=k_b=1.0\times10^{-12}$ N m; dashed lines: $k_l=k_b=1.0\times10^{-13}$ N m.

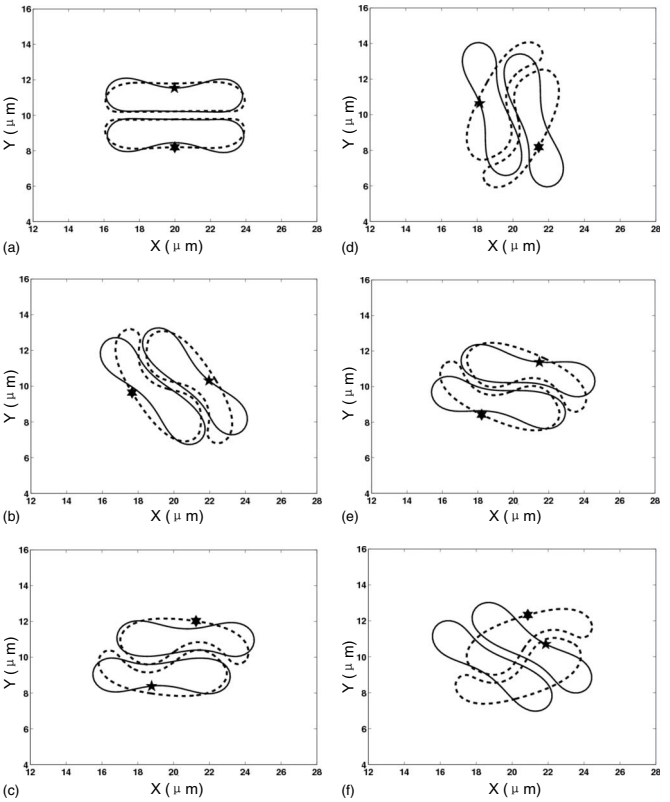

FIG. 7. Representation snapshots for the evolution of rouleaux of two cells in a shear flow with $\gamma=100\ s^{-1}$. (a) $t=0$, (b) $\gamma t=5$, (c) $\gamma t=10$, (d) $\gamma t=15$, (e) $\gamma t=20$, and (f) $\gamma t=75.8$. The intercellular interaction between the two cells is strong with $D_e=1.0\ \mu J/m^2$. Solid lines: $k_l=k_b=1.0\times10^{-12}$ N m; dashed lines: $k_l=k_b=1.0\times10^{-13}$ N m.

RBC very well. The biconcave cells obtained with $s^*=0.481$ will be used for the simulation of the two-cell rouleaux.

After obtaining the shape of the RBCs for a given area reduction ratio, such RBC shape is put into a $20\times20\ \mu m^2$ domain to obtain its equilibrium shape in a static plasma. For the results shown in this paper, the coupled RBC motion and fluid flow is solved by the immersed boundary method based on the Navier-Stokes equations with the force given in Eq. (13). The elastic force induced by the springs is substituted into the Navier-Stokes equations as a body force. The equilibrium shapes shown in Fig. 2 demonstrate that the RBCs simulated by elastic spring model are stable in blood plasma.

B. Simulation of single cell

Tank treading of the RBC membrane in a simple shear flow has been observed experimentally by Fischer *et al.* [7] and many others, e.g., [16]. It was observed that at equilibrium, although the global shape of the RBC is stationary, the membrane circulates along the contour such as a tank tread with the cell orientating to a fixed inclination angle. It was also found that the tank-treading frequency depends on the shear rate and the viscosity of the surrounding viscous fluid [7]. In Fig. 3, the elastic spring model is validated by comparing with previous experimental data [7], theoretical Keller and Skalak model [17], and simulations [18,19] for the inclination angles and tank-treading frequencies of single RBCs in shear flows. From Fig. 3, it can be seen that our simulation results agree very well with those in [18] for the inclination angles. It is also noted that our results for the tank-treading frequency has the same linear behavior as that of the experiment [7] and is with less discrepancy than the simulation results obtained by Li *et al.* [19]. We also keep track of the cell area and perimeter during the simulations. The change is less than $\pm0.1\%$ in the area and less than $\pm0.5\%$ in the perimeter.

C. Simulation of two-cell rouleaux

It has long been recognized that RBCs can aggregate to form stacks-of-coins-like rouleaux (aggregates). In this section, we first investigate the formation of the RBC rouleaux under no-flow condition to eliminate the influence of the hydrodynamic viscous forces. Two biconcave-shaped RBCs with intercellular forces are placed in static blood plasma for them to aggregate as shown in Fig. 4(a). The simulations have been done in a $20\times20\ \mu m$ domain. The distance between the centers of the two RBCs is 3.1 μm so that the intercellular force is attractive initially. As time elapses, the RBCs move toward each other until the balance of the attractive force and the repulsive force is reached. The equilibrium

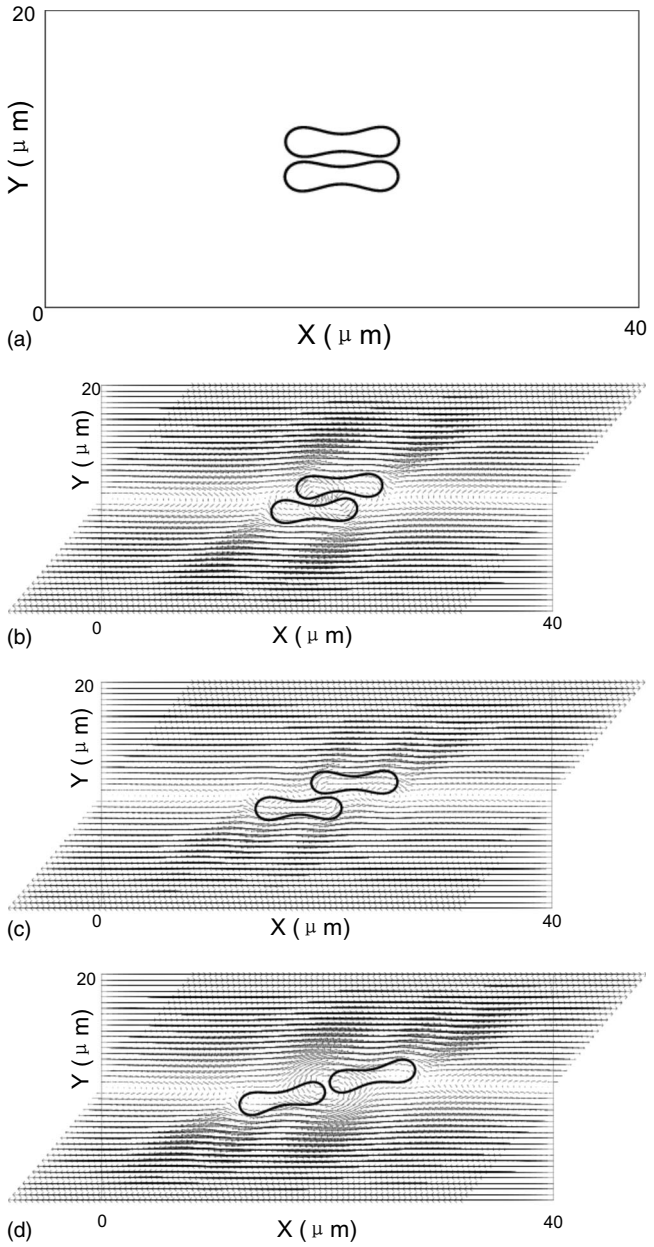

FIG. 8. Snapshots of the dissociation of RBC rouleau in a shear flow with $\gamma=750^{-1}$ for the case of $D_e=1.0\times10^{-2}$ μJ/m^2. The membrane constants $k_l=k_b=1.0\times10^{-13}$ N m. The time instants are: (a) $t=0$ (initial state), (b) $\gamma t=1.5$, (c) $\gamma t=3.75$, and (d) $\gamma t=5.625$.

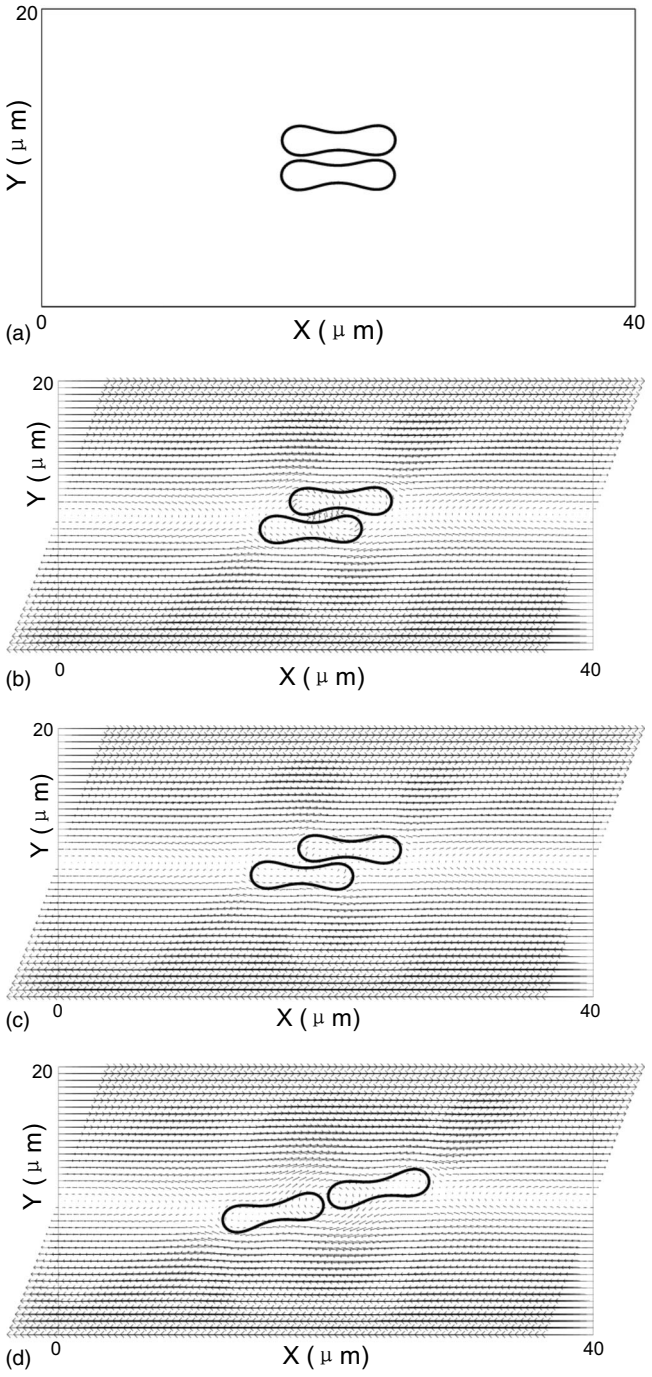

FIG. 9. Snapshots of dissociation of the RBC rouleau in a shear flow with $\gamma=350^{-1}$ for the case of $D_e=1.0\times10^{-2}$ μJ/m^2. The membrane constants $k_l=k_b=1.0\times10^{-13}$ N m. The time instants are: (a) $t=0$ (initial state); (b) $\gamma t=1.75$; (c) $\gamma t=3.5$; (d) $\gamma t=7$.

shape of the rouleaux as a function of D_e are plotted in Figs. 4(b)–4(f) for two types of cells with different spring constants: more deformable cells with $k_b=k_l=1.0\times10^{-13}$ N m and less deformable cells with $k_b=k_l=1.0\times10^{-12}$ N m. The equilibrium shapes of the cells clearly demonstrated that the intercellular interaction is a crucial factor for the deformation of the RBC cells in aggregation process. We also observed that the more rigid cells display concave shapes for all intercellular strengths. For the more deformable cells, the cells display concave shapes at weak intercellular strengths, flattened shapes at moderate intercellular strength, and convex shape at strong intercellular strength. Moreover, we observe curved contact surfaces between two cells at lower intercellular energies and flat contact surfaces at higher D_e values. Note that Zhang *et al.* [6] also did a similar simulation on four-cell rouleaux without consideration of the effect of the deformability and the above results qualitatively agree with theirs.

The behaviors of the RBC aggregates in flows are more complex than single RBCs for the interaction between the cells affects the flow rheology significantly. The rouleaux

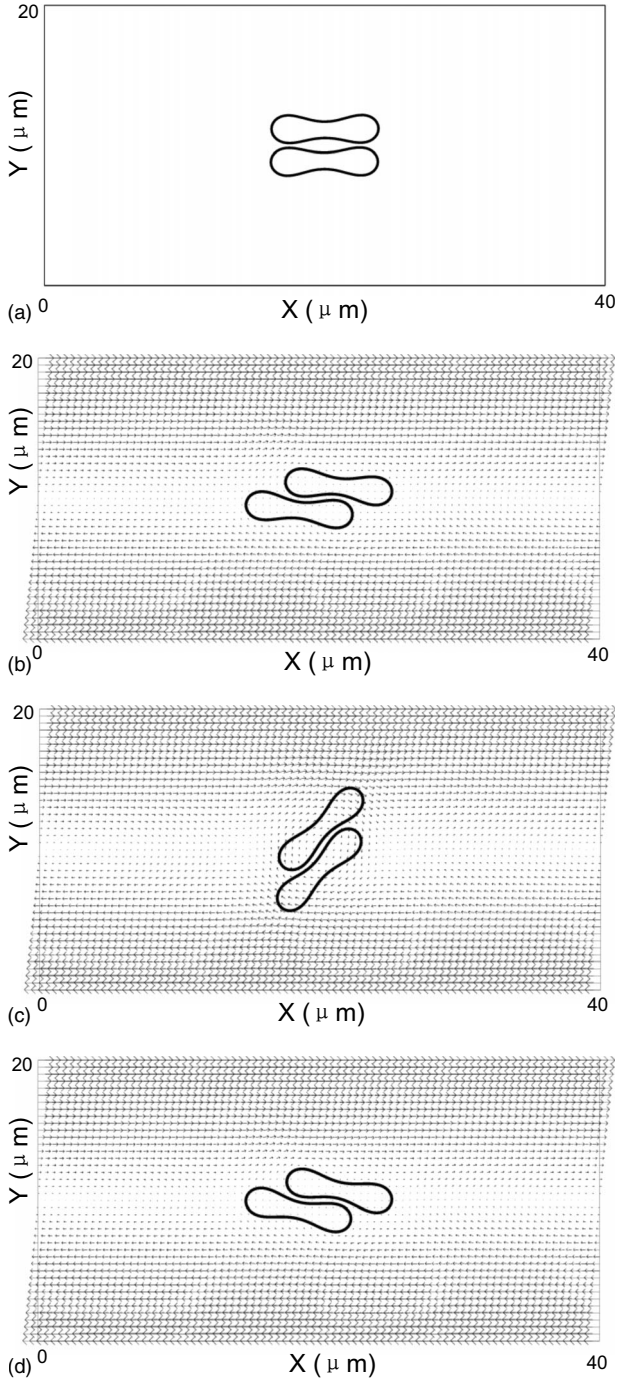

FIG. 10. Snapshots of dissociation of the RBC rouleau in a shear flow with $\gamma=100^{-1}$ for the case of $D_e=1.0\times10^{-2}$ $\mu J/m^2$. The membrane constants $k_l=k_b=1.0\times10^{-13}$ N m. The time instants are: (a) $t=0$ (initial state); (b) $\gamma t=5$; (c) $\gamma t=20.6$; (d) $\gamma t=30.1$.

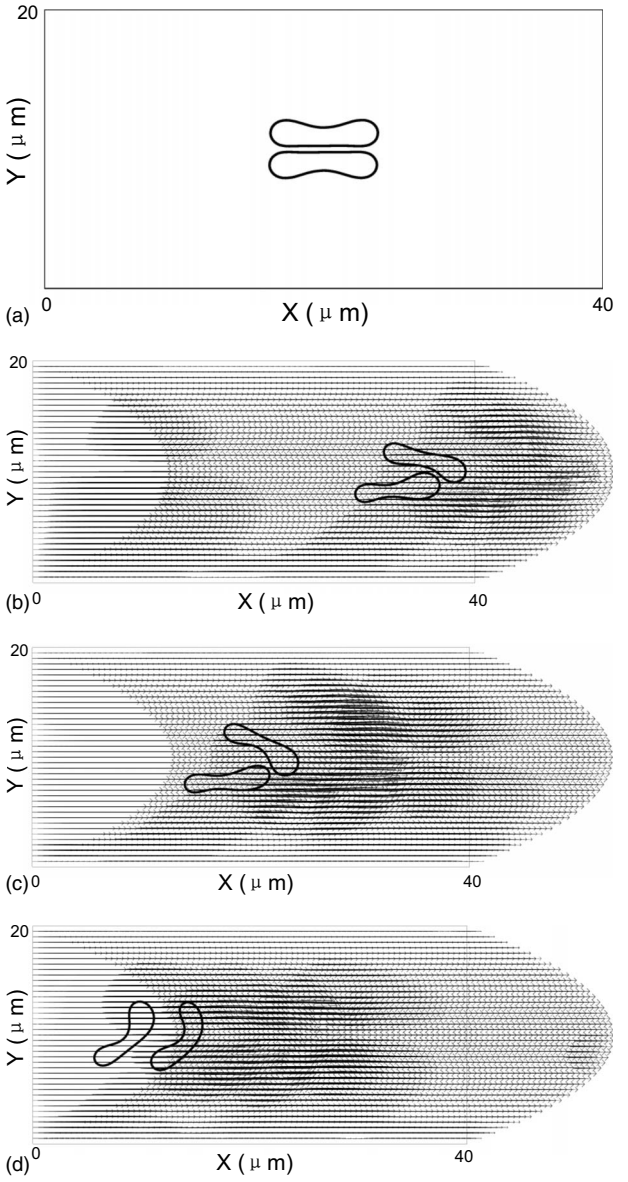

FIG. 11. Snapshots of dissociation of RBC rouleau in a Poiseuille flow with Re=3.4 for the case of $D_e=1.0\times10^{-1}$ $\mu J/m^2$. The membrane constants $k_l=k_b=1.0\times10^{-13}$ N m. The time instants are: (a) $t=0$ (initial state); (b) $t=2$ ms; (c) $t=2.5$ ms; (d) $t=5$ ms.

formed under no-flow condition, as described above, are placed in shear flows to investigate the motion and dissociation of the aggregates. The flow domain considered is a 40×20 μm^2 channel. The rouleaux are located at the center of the domain initially. As the flow starts, the rouleaux move, deform, or even detach depending on the strength of the hydrodynamic viscous force, intercellular force, and the mechanical properties of the membrane. Results at higher constants $k_l=k_b=1.0\times10^{-12}$ N m and lower constants $k_l=k_b=1.0\times10^{-13}$ N m are shown in the same plot in Figs. 5–7 for easy comparison. In addition, two points with one on the upper less deformable cell surface and the other on the lower more deformable cell surface are marked to show the tank-treading motion of the cell membrane. In these three figures, we focus our attention on the deformation, configuration, and the tank treading of the cells. Therefore, only the shape behavior of the RBCs is provided.

Figure 5 shows the breakage of the rouleaux when the intercellular force is weak ($D_e=1.0\times10^{-3}$ $\mu J/m^2$). The rouleau formed under no-flow condition in this case is loose with the deformation of the RBCs being small. A shear flow with a shear rate $\gamma=100$ s^{-1} is applied to the rouleaux. Several snapshots are shown for the position and the shape of the

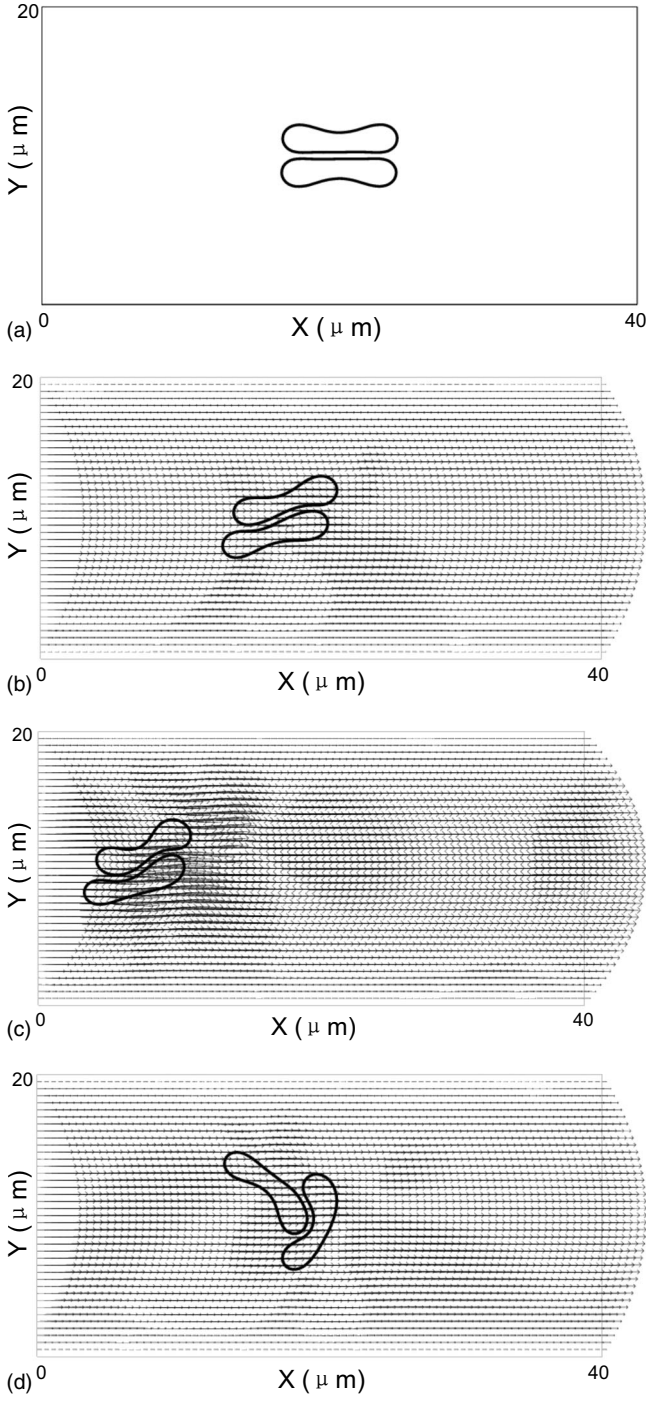

FIG. 12. Snapshots of dissociation of RBC rouleau in a Poiseuille flow with Re=0.83 for the case of $D_e=1.0\times10^{-1}$ μJ/m^2. The membrane constants $k_l=k_b=1.0\times10^{-13}$ N m. The time instants are: (a) $t=0$ (initial state); (b) $t=2$ ms; (c) $t=2.5$ ms; (d) $t=5$ ms.

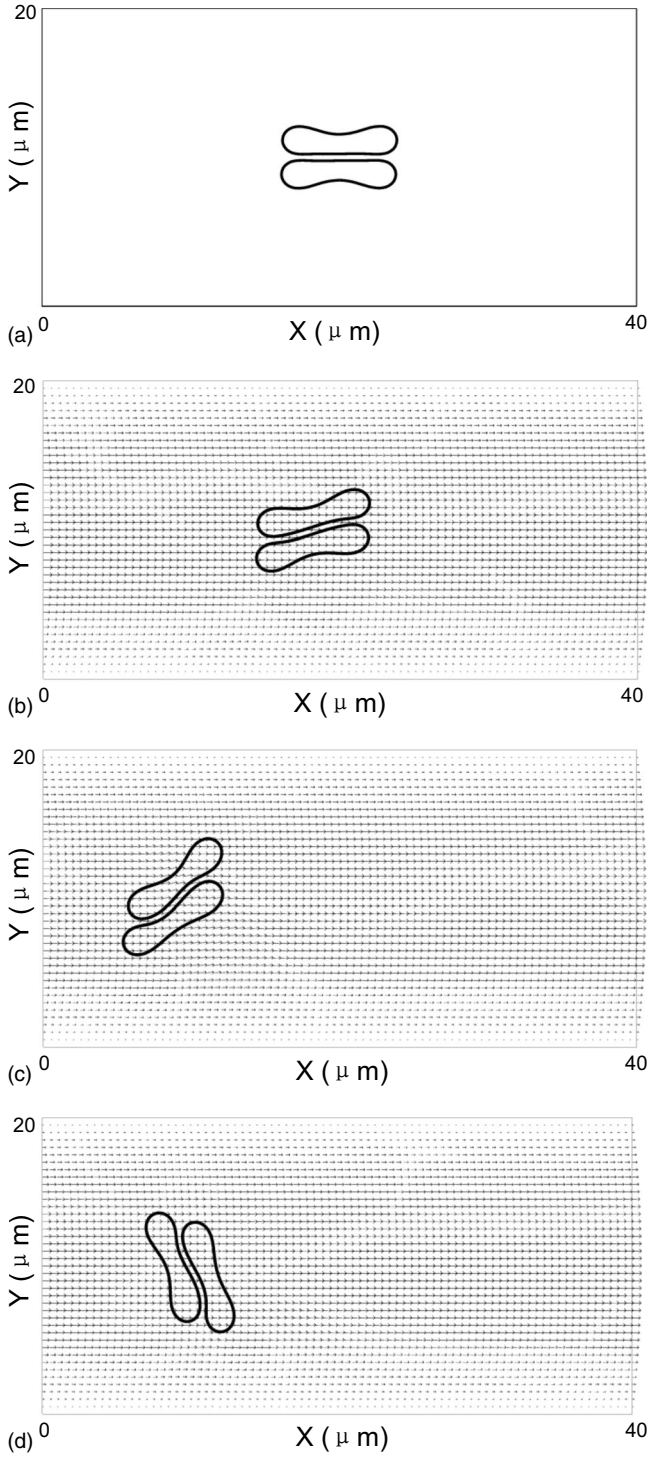

FIG. 13. Snapshots of dissociation of RBC rouleau in a Poiseuille flow with Re=0.17 for the case of $D_e=1.0\times10^{-1}$ μJ/m^2. The membrane constants $k_l=k_b=1.0\times10^{-13}$ N m. The time instants are: (a) $t=0$ (initial state); (b) $t=3$ ms; (c) $t=12$ ms; (d) $t=23.4$ ms.

rouleaux at time $t=0$ and three time instants $\gamma t=1$, 2, and 5. The assemblies detach very quickly to two separate cells. The cells moved to the same direction as the nearby wall with an inclination angle. The two marked points on the cell surface clearly show that the membrane undergoes a tank-treading motion similar to the single cell case. The elasticity of the cell membrane does not have much effect on the behavior of the rouleaux when the intercellular force is weak.

When the intercellular force is moderate ($D_e=1.0\times10^{-1}$ μJ/m^2), the deformation of the RBCs in the rouleaux is also small. When a shear flow with a shear rate $\gamma=100$ s^{-1} is applied to the rouleaux, the two cells slide to the

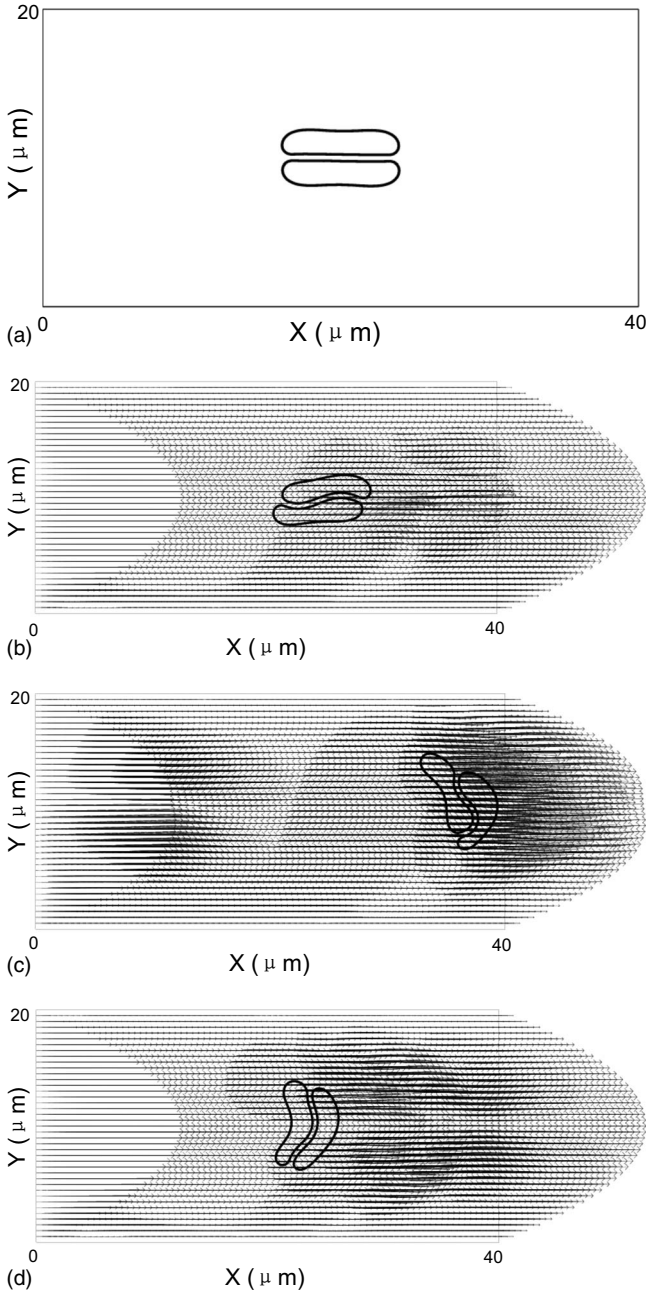

FIG. 14. Snapshots of dissociation of RBC rouleau in a Poiseuille flow with Re=3.4 for the case of $D_e=1.0\ \mu\mathrm{J/m^2}$. The membrane constants $k_l=k_b=1.0\times10^{-13}$ N m. The time instants are: (a) $t=0$ (initial state); (b) $t=1$ ms; (c) $t=5$ ms; (d) $t=141$ ms.

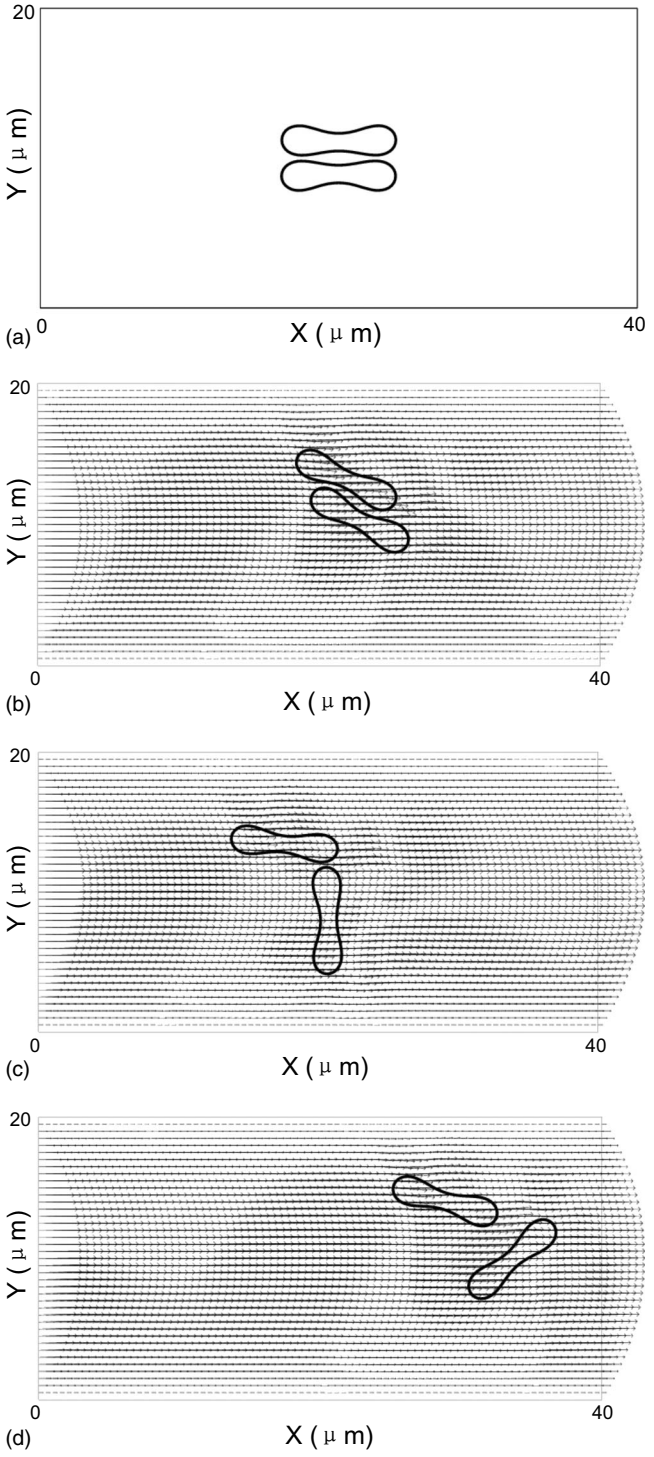

FIG. 15. Snapshots of dissociation of RBC rouleau in a Poiseuille flow with Re=0.83 for the case of $D_e=1.0\times10^{-1}\ \mu\mathrm{J/m^2}$. The membrane constants $k_l=k_b=1.0\times10^{-12}$ N m. The time instants are: (a) $t=0$ (initial state); (b) $t=0.6$ ms; (c) $t=1.6$ ms; (d) $t=2.5$ ms.

opposite direction depending on the direction of the shear flow. However, the hydrodynamic viscous force is not strong enough to break the rouleaux completely. The rouleaux rotate like a single body, keeping the relative position of the two cells unchanged. In Fig. 6, several snapshots are shown for the position and the shape of the rouleaux at time $t=0$ and five time instants $\gamma t=5$, 10, 15, 20, and 77.8. Note that the more deformable cells rotate faster than the less deformable cells. Also, the rotation velocity of the rouleau formed by the more deformable cells is almost constant, while that of the less deformable cells are not. Tank treading has been found for both types of the cells with the velocity being faster for less deformable cells, and the overall tank-treading velocity is slower compared to the weak strength case.

When a strong intercellular force is introduced ($D_e=1.0\ \mu\mathrm{J/m^2}$), the RBCs experience large deformation during the process of rouleaux formation. Moreover, the rouleau

formed is compact with the biconcave shape completely lost for the more deformable cells. Figure 7 shows a shear flow with a shear rate $\gamma=100\ s^{-1}$ being applied to the rouleaux and several snapshots for the instant position of the rouleaux in the flow. For the more deformable cells, the contact surface between the two cells becomes highly curved as the flow starts. Both types of aggregates do not break and roll almost like a single rigid body. Consequently, the tank-treading motion of an individual cell in the rouleau is not present any more. The trace of a point on the cell surface indicates almost no tank treading of the membrane.

To examine the hydrodynamic effect on cell behavior, we place the two-cell rouleaux formed at $D_e=1.0\times10^{-2}\ \mu J/m^2$ in shear flows with varying shear rates (Figs. 8–10). The cells have the bending and stretching or compressing constants $k_l=k_b=1.0\times10^{-13}$ N m. Several snapshots are shown for the position and the shape of the rouleaux at time $t=0$ and three other time instants. When $\gamma=750\ s^{-1}$ is applied to the rouleau, the assembly detaches very quickly to two separate cells and arranges at parallel layers. The cells moved to the same direction as the local fluid with an inclination angle. This angle is found to be the same as in the tank treading. The behavior of the rouleau in a flow with shear rate $\gamma=350\ s^{-1}$ (Fig. 9) is similar to the $\gamma=750\ s^{-1}$ case, however with a slower detaching of the cells. In a flow with $\gamma=100\ s^{-1}$ (Fig. 10), unlike the other two cases, the rouleau does not break. As the flow starts, the cells quickly slide depending on the flow direction. Then the cells rotate together almost like a single rigid body. In Figs. 8–10, the vector field of the flow velocity is also provided in the same plot. As the cell moves, the fluid flow around the cells is not linear shear flow because of the interaction between the cells and the plasma.

To study the dynamical RBC behavior in Poiseuille flows, the two-cell rouleaux formed at intercellular strength $D_e=1.0\times10^{-1}\ \mu J/m^2$ are placed in Poiseuille flows with varying Reynolds numbers at the inlet. The flow domain considered is a $40\times20\ \mu m^2$ channel with the rouleaux locating at the center of the domain initially. In the flow, the rouleaux move with the plasma while experiencing deformation. The rouleaux can even become individually dispersed depending on the hydrodynamic viscous force and the mechanical properties of the membrane. Results at three different inlet Reynolds numbers Re=3.4, 0.83, and 0.17 are shown in Figs. 11–13 for the evolution of the rouleaux formed with more deformable cells ($k_l=k_b=1.0\times10^{-13}$ N m). At the two higher inlet Reynolds numbers, the rouleaux can be dissociated into two separate cells. The higher the Reynolds number, the faster the disaggregation. However, when the inlet Reynolds number is 0.17, the hydrodynamic force produced by the flow is not strong enough to break the assembly. Another experiment with the inlet Re=3.4 is carried out on the rouleau with a stronger intercellular strength $D_e=1.0\ \mu J/m^2$ (Fig. 14). Compared to the case shown in Fig. 11, the rouleau simply deforms and rotates in the flow and cannot be broken due to this strong interaction. In Fig. 15, a rouleau formed with rigid cells (i.e., strong bending constant $k_l=k_b=1.0\times10^{-13}$ N m) is placed in a Poiseuille flow with inlet Re=0.83. The interaction force is $D_e=1.0\times10^{-1}\ \mu J/m^2$, the same as in Fig. 11. It is noted that the cells with weak bending constant (Fig. 11) are more difficult to break in the flow. On the other hand, the assembly with strong bending (Fig. 15) is more likely to disaggregate into individual cells. In Figs. 11–15, the vector fields provided for the fluid flow clearly show the effect of the cell-cell and cell-fluid interactions on the flow rheology. It is also noted that the parachute shape of RBCs, which has been observed under physiological conditions, has been found in some of the above Poiseuille flows (see Figs. 11, 12, and 14).

The above simulations show that in microchannels, the behaviors of RBC rouleaux are strongly related to the deformability of the membrane, the strength of the intercellular interaction, and the hydrodynamic force induced by the flow. Experiments show that RBC rouleaux can be broken into individual cells at higher hydrodynamic forces, which are induced by higher shear rate in shear flow or higher Reynolds number in the Poiseuille flow, or weak intercellular strength. It is also noted that in the Poiseuille flows, increase in the rigidity of the cell membrane will facilitate the disassociation of the rouleaux. It indicates that the rheological motion of the RBCs is the result of a balance between aggregating and dissociating forces.

IV. CONCLUSIONS

In summary, a numerical model is developed to investigate the aggregation of RBCs and the dissociation of the RBC rouleaux in microvessels. An elastic spring model is adopted to describe the cell membrane. Based on the available mechanical properties of RBCs, cells have been studied using a two-dimensional approximation. The equilibrium configuration of rouleaux formed under the action of intercellular interaction is related to the strength of the intercellular force and the deformability of the cell membrane. The cells in the rouleaux exhibit the typical biconcave shapes, flatten shapes, or even convex shapes. In shear and Poiseuille flows, such a rouleaulike aggregate will rotate or to be separated, depending on factors such as shear stress, the strength of the intercellular interaction and the deformability of the membrane. These factors are investigated in this paper for their effects on the deformation and motion of RBC rouleaux in channel flows, and the results show the significant influence of these factors on the rheological properties and motion of the RBCs in microvessels. The tank-treading behavior has also been found for the individual cells in the rouleaux with weak or moderate intercellular strength. In addition, the numerical results are quantitatively/qualitatively similar to experimental observations and other investigators' findings, thus showing the potential of this numerical algorithm for future studies of blood flow in microcirculation.

ACKNOWLEDGMENTS

The authors acknowledge the support of NSF (Grants No. ECS-9527123, No. CTS-9873236, No. DMS-9973318, No. CCR-9902035, No. DMS-0209066, and No. DMS-0443826).

[1] T. W. Secomb, in *Modeling and Simulation of Capsules and Biological Cells*, edited by C. Pozrikidis (Chapman and Hall/CRC, Boca Raton, FL, 2003).
[2] A. Borhan and N. R. Gupta, in *Modeling and Simulation of Capsules and Biological Cells*, edited by C. Pozrikidis (Chapman and Hall/CRC, Boca Raton, 2003).
[3] P. Bagchi, P. C. Johnson, and A. S. Popel, J. Biomech. Eng. **127**, 1070 (2005).
[4] Y. Liu, L. Zhang, X. Wang, and W. K. Liu, Int. J. Numer. Methods Fluids **46**, 1237 (2004).
[5] Y. Liu and W. K. Liu, J. Comput. Phys. **220**, 139 (2006).
[6] J. Zhang, P. C. Johnson, and A. S. Popel, J. Biomech. **41**, 47 (2008).
[7] T. M. Fischer, M. Stöhr-Liesen, and H. Schmid-Schönbein, Science **202**, 894 (1978).
[8] J. C. Hansen, S. Skalak, and A. Hoger, Biophys. J., **70**, 146 (1996).
[9] C. Vera, R. Skelton, F. Bossens, and L. A. Sung, Ann. Biomed. Eng. **33**, 1387 (2005).
[10] K. Tsubota, S. Wada, and T. Yamaguchi, Journal of Biomechanical Science and Engineering **1**, 159 (2006).
[11] A. S. Popel and P. C. Johnson, Annu. Rev. Fluid Mech. **37**, 43 (2005).
[12] H. Baumler, B. Neu, E. Donath, and H. Kiesewetter, Biorheology **36**, 439 (1999).
[13] C. S. Peskin, J. Comput. Phys. **25**, 220 (1977).
[14] B. Chung, P. C. Johnson, and A. S. Popel, Int. J. Numer. Methods Fluids **53**, 105 (2007).
[15] E. A. Evans and Y. C. Fung, Microvasc. Res. **4**, 335 (1972).
[16] R. Tran-Son-Tay, S. P. Sutera, and P. R. Rao, Biophys. J. **46**, 65 (1984).
[17] S. R. Keller and R. Skalak, J. Fluid Mech. **120**, 27 (1982).
[18] J. Beaucourt, F. Rioual, T. Séon, T. Biben, and C. Misbah, Phys. Rev. E **69**, 011906 (2004).
[19] H. B. Li, H. H. Yi, X. W. Shan, and H. P. Fang, EPL **81**, 54002 (2008).